Electron Reflectometry for Measuring Nanostructures on Opaque Substrates

Lawrence H. Friedman[1, a] and Wen-Li Wu[2]

[1] *National Institute of Standards and Technology, Materials Measurement Science Division, Gaithersburg, MD 20910, United States of America*

[2] *National Institute of Standards and Technology, Materials Science and Engineering Division, Gaithersburg, MD 20910, United States of America*

Here, we present a method for measuring dimensions of nanostructures using specular reflection of electrons from an electronically opaque surface. Development of this method has been motivated by measurement needs of the semiconductor industry[1–4], and it can also be more broadly applicable to any periodic, pseudo-periodic or statistically stationary nanostructures or nanopattern on an opaque substrate. In prior work[5,6], it was demonstrated through the presentation of proof of concept experiments and simulated examples that Reflective Small Angle Electron Scattering (RSAES) can meet certain dimensional metrology requirements of the semiconductor industry. In RSAES, an entire reflected scattering pattern is measured, with the scattered electrons being of primary interest. Later, in the process of further simulating RSAES, it was serendipitously discovered that dimensional measurement using reflected electrons might be greatly simplified by Electron Reflectometry (ER), whereby the intensity of the specularly reflected electron beam is measured and the scattered beams ignored.[7] This innovation may allow faster and cheaper development and deployment or at the very least provide an alternate pathway to exploit the phenomenon of reflected electrons for dimensional measurement. Here we discuss how ER complements existing dimensional measurement techniques, show simulated applications with an emphasis an defect detection and line-width measurements.

[a] Electronic mail: lawrence.friedman@nist.gov

Dimensional metrology needs of the electronics and semiconductor industry[1–4] are primarily addressed through the techniques of X-Ray scattering[8,9], optical scatterometry (or optical critical dimension metrology, OCD)[3,10], scanning and transmission electron microscopy (SEM and TEM), and scanning probe microscopy (SPM). Each technique has its advantages and disadvantages, but electron reflection may be well suited for measuring three-dimensional features smaller than 10 nm with: (1) high dimensional precision, (2) measurement footprint with linear dimension smaller than $100\,\mu$m, (3) little to no sample preparation, (4) strong output signal. Furthermore, when used in a hybrid measurement scheme, it is anticipated that RSAES and ER will serve to resolve parameter cross-correlation[1,3,4] because of their strong response to surface geometry. For more discussion see Ref.[5] on RSAES. Existing and new dimensional measurement techniques continue to be modified and further developed.[4,9,11].

The benefits of electron reflection methods (RSAES and ER) come from the large scattering cross-section of electrons that are approximately 10^8 times larger than X-ray cross-sections[12], the abilities to focus, deflect, vary the energy of and filter electrons, and the availability of a variety of compact sources and detectors. In ER, an incident electron beam of energy 5 keV to 100 keV is scanned through various angles relative to a sample, and the specularly reflected beam intensity is measured. While rocking Reflective High Energy Electron Diffraction (rocking-RHEED) has been used to measure atomic-scale features such as adatom step-size and coverage,[13] ER measures nanoscale dimensions with a controllable beam footprint.

Reflectance measurement is proposed using the schematic in Fig. 1. Caps are used for sample coordinates ($X-Y-Z$), and lower-case is used for instrument coordinates ($x-y-z$). The incident electron beam and detected detected electron beam lie in the reflection-plane (instrument $x-z-$plane). The reflection measurement angle (θ_r) is between the incident beam and the instrument $x-y-$plane. The detection direction has the same angle with the $x-y-$plane, θ_r. Using the instrument coordinates and starting from alignment of the sample with the instrument, the final sample orientation can be defined by a sequence of active rotations: first, rotate sample about instrument $z-$axis by azimuthal angle (ϕ); second, rotate sample about instrument $y-$axis by pitch angle (θ); third, rotate sample about instrument $x-$axis by the roll angle (β). ER can measure sample features by recording electron reflectance while scanning through the various angles.

The ability of ER to measure nanoscale shape and defects is demonstrated through simulated measurement of a typical test grating that has pitch (P), height (H), width (W), sidewall angle (θ_sw). Considered defects include top-rounding of radius, ρ_tr, and undercut of radius, ρ_uc (Fig. 2).

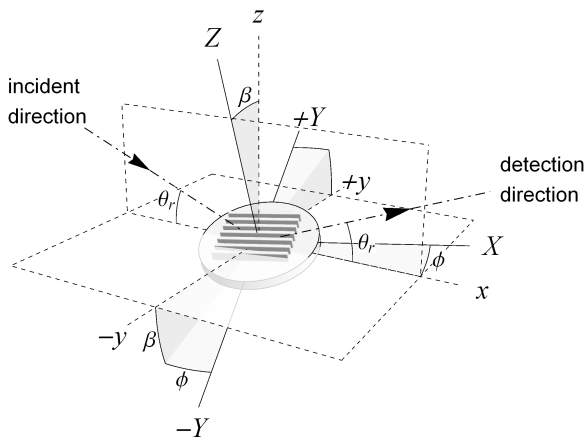

Figure 1. Coordinate system and angles of electron reflectance measurement. X,Y,Z are sample coordinates, while x,y,z are instrument coordinates. y-plane is shown as semi-transparent square with dashed edges. Nominal reflection plane $(x-z)$ is indicated with transparent dashed rectangle. Also shown: reflection measurement angle (θ_r), roll angle (β), and azimuthal (yaw) angle (ϕ). Pitch angle (θ) is zero and not shown.

Grating lines run along the sample X-direction and transverse to the Y-direction. The Z-direction is normal to the substrate.

Fig. 2 also shows a simulated electron probability density during reflection with small azimuthal rotation. Wave functions were simulated using the previous method[5,13,14] but now implemented in Python.[15] Electrons have wavelength, $\lambda_e = 9.94$ pm (accelerating voltage = 15 kV), and the grating and substrate have a mean inner potential for Si[16] $U = (-12.1 - i2.23)$ eV. The imaginary part is a first approximation to inelastic scattering. Simulations were refined until converged with no perceptible impact of increased refinement; simulations included 129 Fourier components in the horizontal direction and a discretization of 4 Å^{-1} in the vertical direction. The ability of ER to detect certain minute defects such as top rounding and undercut is illustrated by the change in electron wave function in and around these defects and consequently, the far-field electron current density. Contrast the wave-functions in Figs. 2a and 2b (Multimedia view). This difference, even in the free-space above the grating, illustrates how small changes in the sample geometry have visible impact on the reflected wave-function and ultimately on the detected current as the wave continues to propagate away from the sample. Fig. 2b (Multimedia view) further demonstrates this phenomenon as grating geometry is varied continuously with the consequent variations in electron wave-function and reflectance shown.

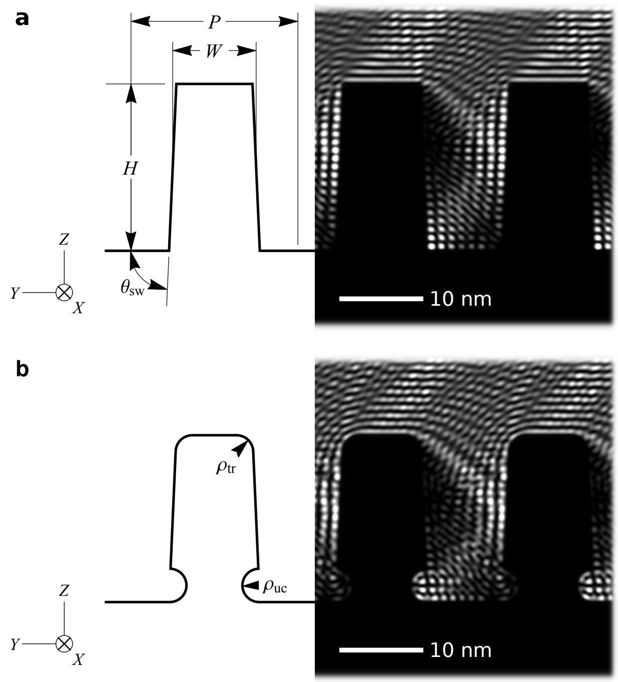

Figure 2. Hypothetical test grating with example simulated electron probability density (PDF) during reflection. Shading is from PDF = 0 (black) to PDF = 4 (white). Incident wave is normalized to PDF = 1. Simulated incident beam has wavelength, $\lambda_e = 9.94$ pm and reflection measurement angle, $\theta_r = 0.3°$. Sample orientation is $(\phi, \theta, \beta) = (0.2°, 0°, 0°)$. (a) As drawn and simulated, $P = 20$ nm, $H = 20$ nm, $W = 10$ nm, $\theta_{sw} = 87.5°$. (b) As Fig. a, but with top-rounding ($\rho_{tr} = 2.0$ nm) and undercut ($\rho_{uc} = 2.0$ nm). Differenct cases of grating geometry are simulated responding to the same incident beam with resulting electron wave function and reflectance (R) shown. (Multimedia view)

Three models of electron reflectance are used to predict reflectance measurements from the proposed method. First, optical path differences (OPDs) are used to elucidate how ER is sensitive to grating height (H), pitch (P) and undercut (ρ_{uc}). This kinematic analysis, however, serves only as a guide to understanding. In contrast to interpreting data from X-ray diffraction methods where scattering is often well described by kinematic theories, electron reflection involves multiple (dynamic) scattering. Second, dynamic scattering simulations of idealized ER angle scans are presented. Finally, more realistic simulations are presented that takes into account beam decoherence and finite angular width and use modeling parameters inspired by currently available electron optical components.

Now, consider OPD analysis of various angular scans. A scan with varying reflection measurement angle (θ_r), with all other angles zero, results in an optical path difference between the top

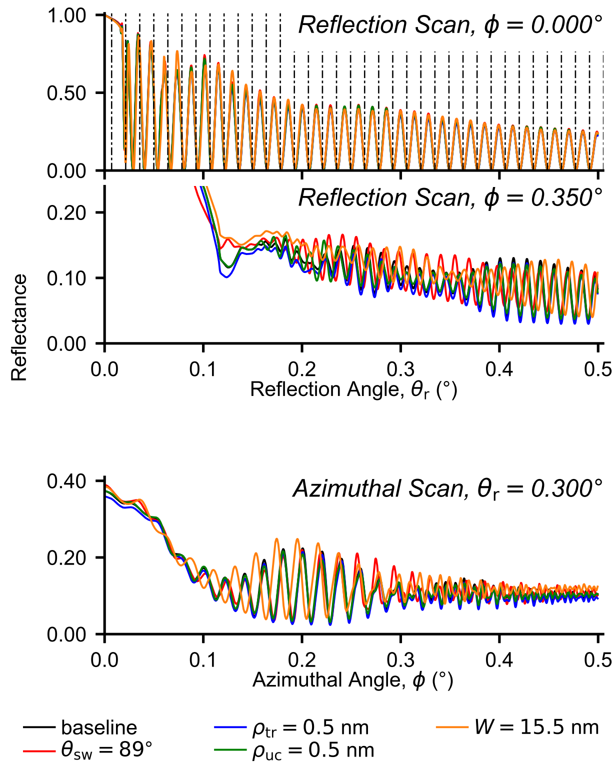

Figure 3. Dynamic simulations of ER scans of baseline and other gratings as described in text assuming perfect incident beam and detector collimation. Baseline grating dimensions (see Fig. 2a) are $P = 30$ nm, $H = 20$ nm, $W = 14.5$ nm, and $\theta_{sw} = 88°$. Non-baseline simulations are as described in text and legend (see Fig. 2b). Vertical dot-dashed lines indicate OPD-predicted reflectance minima.

of the grating and the substrate, $OPD = (2\pi/\lambda_e) \times 2H \sin\theta_r$. Intensity minima are expected when $\sin\theta_r = (\lambda_e/4H)(2n+1)$. Similarly, an azimuthal scan in (ϕ) with fixed reflection measurement angle (θ_r) and zero pitch and roll angle ($\theta = \beta = 0$) measures pitch (P) with an optical path difference given by $OPD = (2\pi/\lambda_e)\cos\theta_r \times 2P\sin\phi$. Reflected intensity minima are anticipated when $\sin\phi = (\lambda_e \sec\theta_r/4P)(2n+1)$. Other geometric features are should modulate the electron reflection intensity, but not in ways that can be described simply. For example, it is expected that scans will be sensitive to undercut when an electron probability peak fits inside, $(\lambda_e/2)\csc\theta_r \leq 2\rho_{uc}$ or $\sin\theta_r \geq \lambda_e/(4\rho_{uc})$. To scan for undercut of radius of 0.5 nm, a reflection measurement angle, $\theta_r \geq 5$ mrad (0.29°) would seem advisable.

Dynamic simulations provide more accurate and precise prediction of ER and can test the efficacy of OPD analysis. ER is simulated for a baseline grating ($P = 30$ nm, $H = 20$ nm, $W = 14.5$ nm, and $\theta_{sw} = 88°$) and then for four distinct variations about this base configuration: $W \rightarrow 15.5$ nm; $\theta_{\mathrm{sw}} \rightarrow 89^{\circ}$; $\rho_{\mathrm{tr}} \rightarrow 0.5$ nm; finally, $\rho_{\mathrm{uc}} \rightarrow 0.5$ nm, similar to the simulations in Fig. 2b (Multimedia view). As before, electron wavelength is $\lambda_{\mathrm{e}} = 9.94$ pm, and grating/substrate potential is $U = (-12.1 - i2.23)$ eV. Reflectances are simulated and plotted for perfectly collimated incident beam and detector, *i.e.* zero angular width (Fig. 3).

The first simulation is a reflection scan with azimuth (ϕ) set to 0°, and reflection measurement angle (θ_{r}) is varied from 0° to 0.5°. The simulated reflectance approaches $R = 1$ at $\theta_{\mathrm{r}} = 0^{\circ}$, and then decays and oscillates as θ_{r} increases with period similar to that predicted by OPD analysis for grating height, with minima slightly shifted from $\theta_n = \sin^{-1}\left[\left(1.24 \times 10^{-4}\right) \times (2n+1)\right]$, when $\theta_{\mathrm{r}} > 0.1^{\circ}$. There is, however, no separation between the various reflectance curves indicating that the $\phi = 0^{\circ}$ reflection scan is useful for height measurement, but not necessarily for defect detection or geometric variation.

The second simulation is a reflection scan that is off-azimuth with constant $\phi = 0.350^{\circ}$. The reflectance has an irregular pseudo-period similar to that of the $\phi = 0^{\circ}$ scan when $\theta_{\mathrm{r}} > 0.220^{\circ}$, thus retaining some height information. More importantly, the various reflectance curves are somewhat separated so that the off-azimuth reflection scan can potentially measure the four types of variations discussed.

The third simulation is an azimuthal scan where $0^{\circ} < \phi < 0.5^{\circ}$ as reflection measurement angle is held constant at $\theta_{\mathrm{r}} = 0.300^{\circ}$. The resulting reflectance curves oscillate, but there is no obvious period; oscillations accelerate noticeably at higher azimuthal angles. There is, however, distinct separation between the reflectance curves so that the azimuthal scan has potential to detect features of interest.

The scattering geometry of Fig. 1 can be achieved in practice by various means including the apparatus embodiment in Fig. 4. The depicted instrument has a length of about 1.4 m. It has a compound electron lens, a replaceable beam aperture and a set of scanning coils to aim and collimate the incident beam, a manipulable sample stage to help select the area to be measured and position the sample, a second set of scanning coils and a second aperture to control the detection angle and detection angular width, and an electron detector that measures beam current. The incident electron beam can be rocked while keeping the incident footprint stationary. This embodiment and others can be characterized by three figures of merit: angular resolution (α), sample footprint linear dimension ($2a_{\mathrm{fp}}$), and incident electron current (I_{i}). The notation $2a_{\mathrm{fp}}$ is used because a circular aperture and a glancing angle lead to highly elliptical footprint with major axis length of $2a_{\mathrm{fp}}$.

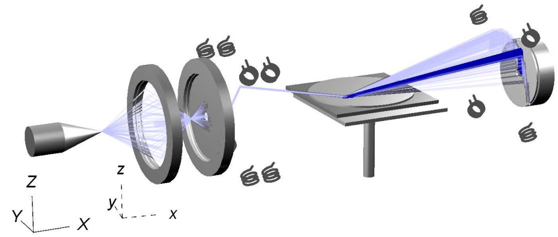

Figure 4. Embodiment of electron reflectometer (angles exaggerated and not to-scale). Blue lines show electron path. Dark blue indicates electron trajectories that contribute to reflectance measurement. In this embodiment, sample axes ($X-Y-Z$) have fixed orientation, and sample orientation is achieved primarily through passive rotation, *i.e.* rotation of instrument axes, $x-y-z$, using scanning coils.

Two configurations are evaluated that use instrument parameters familiar to the SEM community. To keep the instrument length close to 1 m, the working distance and camera length are $l_\mathrm{w} = l_\mathrm{c} = 0.5$ m. Field emission electron guns have brightnesses close to $B = 0.5\times10^{12}$ A srad^{-1}m^{-2}. The electron spot size is focused to $d_\mathrm{s} = 150$ nm transverse to the optical axis. To achieve high resolution, the first configuration uses an incident electron aperture diameter and detection aperture diameter, $d_\mathrm{i} = d_\mathrm{d} = 20\,\mu$m. The second configuration sacrifices angular resolution for enhanced electron current, $d_\mathrm{i} = d_\mathrm{d} = 100\ \mu$m and reduced incident beam footprint. Numerical simulations require a double integral over reflection Green functions that were interpolated over 512 by 512 grid for reflection and azimuthal angles spanning $0°$ to $0.5°$. Additionally, finite size of source images is included as a beam decoherence factor that is only appreciable for very large aperture measurements.

The first design has angular resolution $\alpha = d_\mathrm{i}/(2l_\mathrm{w}) = 2\times10^{-5}$ rad $= 0.001°$ and gives reflectances (Fig. S1) very close to the ideal (Fig. 3). The width along the minor axis of the elliptical incident footprint is calculated to be $2b_\mathrm{fp} = [\left(d_\mathrm{s}\right)^2 + \left(0.6\lambda_\mathrm{e}l_\mathrm{w}/d_\mathrm{i}\right)^2]^{1/2} = 0.34\ \mu$m. For reflecting angle $\theta_\mathrm{r} = 0.2°$, the length along the major axis is $2a_\mathrm{fp} = 2\csc\theta_\mathrm{r}\, b_\mathrm{fp} = 100\ \mu$m. This final value is due to the large Rayleigh broadening without which it would be a mere 42 μm. The resulting incident current is[17] $I_i = \left(\pi^2/16\right)B\,\left(d_\mathrm{i}/l_\mathrm{w}\right)^2 d_\mathrm{s}^2 = 20$ pA. With a detector sensitivity of 1 fA, this configuration would measure reflectances as small as 5×10^{-5}. Loss of angular resolution from sample curvature[13] is negligible, as that effect is completely ameliorated by the controlled incident footprint size. A typical loss of resolution is estimated from the ratio of the footprint size to

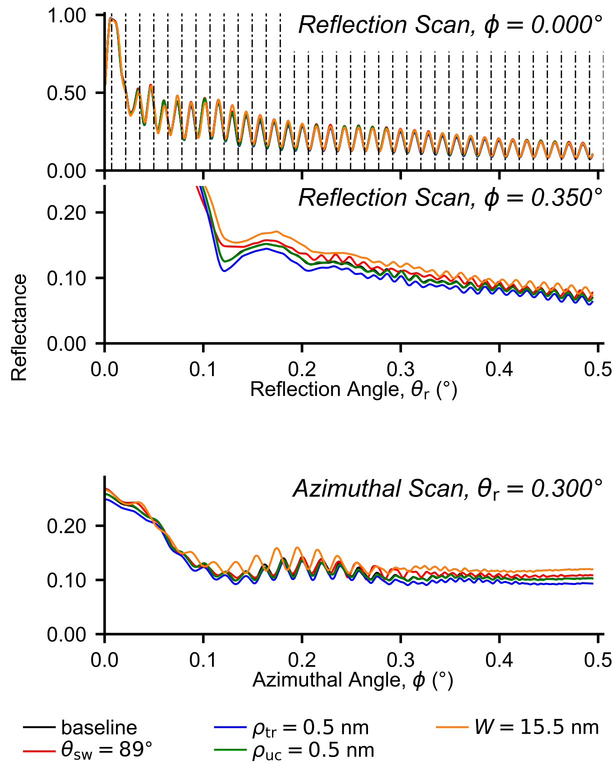

Figure 5. Dynamic simulations of ER scans of baseline and other gratings as in Fig. 3 and described in text, but incident beam and detection aperture diameters are large; $d_\mathrm{i} = d_\mathrm{d} = 100\ \mu$m. Vertical dot-dashed lines indicate OPD-predicted reflectance minima.

typical radius of curvature $\Delta\alpha = (100 \times 10^{-6}\ \mathrm{m})/(100\ \mathrm{m}) = 10^{-8}\ \mathrm{rad} = (6{\times}10^{-7})^\circ$. The average incident current density normal to the sample surface is 8.8 A/m^2, a value of interest if sample damage or charging is a concern.[1,3,4]

The second configuration, with apertures of diameter 100 μm, has angular resolution $\alpha = 10^{-4}\ \mathrm{rad} = 0.006^\circ$. For $\theta_\mathrm{r} = 0.2^\circ$, the footprint length along the major axis is $2a_\mathrm{fp} = 44\ \mu$m, a much smaller value due to the negligible amount of Rayleigh broadening using the larger aperture. The resulting incident current is $I_i = 0.5$ nA. With a detector sensitive to 1 fA, this configuration would measure reflectances as small as 2×10^{-6}. The average normal incident current density is 95 A/m^2. Scans using the larger aperture are shown in Fig. 5. There is some loss of information, but the abilities to observe oscillation periods and detect the presence of defects are retained. Need for a smaller spot size or measurement of samples with a great deal of disorder or significant inelastic scattering may benefit from the enhanced signal and justify the use of larger apertures.

Electron Reflectometry (ER) is a technique for measuring periodic and pseudo-periodic or statistically stationary nanostructures on a substrate that uses the total current of specularly reflected electrons. Electron wave functions and reflectances at small reflection measurement angles depend strongly on surface geometry allowing ER to be used for dimensional measurement of nanostructures. ER is simpler than Reflective Small Angle Electron Scattering (RSAES) as it dispenses with the need for objective electron lenses. ER can measure height as well as undercut, top rounding, sidewall angle differences, and variations in grating line widths, even for widths near 50 % of the pitch. Optical path difference analysis is useful in interpreting height measurements, but in most cases dynamic simulation is needed for prediction and analysis. The ER phenomenon is demonstrated through modeling and simulation of its application to a representative etched Si line grating. Its potential for practical implementation is demonstrated through simulations with parameters typical of contemporary electron optics technology.

SUPPLEMENTARY MATERIAL

See supplementary material for results of dynamic simulations of ER scans with $d_\mathrm{i} = d_\mathrm{d} = 20\,\mu$m, Fig. S1.

ACKNOWLEDGMENTS

Thanks to J. H. Scott for informative discussion. Authors may have some financial rights regarding the allowed patent[18].

REFERENCES

[1] *International Technology Roadmap for Semiconductors 2.0. Metrology* (2015).

[2] A. Vaid, A. Elia, G. Iddawela, C. Bozdog, M. Sendelbach, B. C. C. Kang, P. K. Isbester, and S. Wolfling, J. Micro/Nanolith. MEMS MOEMS **13**, 041410 (2014).

[3] B. Bunday, in *Proc. of SPIE*, Vol. 9778 (2016) pp. 97780E–97780E–34.

[4] B. Bunday, A. F. Bello, E. Solecky, and A. Vaid (SPIE, 2018) pp. 105850I–105850I–44, conference Proceedings.

[5] L. H. Friedman, W.-L. Wu, W.-E. Fu, and Y. Chien, Appl. Phys. Lett. **111**, 123106 (2017).

[6]W.-L. Wu, Y.-S. Chien, W.-E. Fu, Y.-S. Chen, and H.-C. Ho, "United States Patent: 9390888 - Apparatus and method of applying small-angle electron scattering to characterize nanostructures on opaque substrate," (2016).

[7]Lawrence H. Friedman and Wen-Li Wu, "United States Patent Application: Pub. No. 2019/0057834 A1 - Electron Reflectometer and Process for Performing Shape Metrology," (2019).

[8]M. Krumrey, G. Gleber, F. Scholze, and J. Wernecke, Meas. Sci. Technol. **22**, 094032 (2011); T. Hu, R. L. Jones, W.-l. Wu, E. K. Lin, Q. Lin, D. Keane, S. Weigand, and J. Quintana, Journal of Applied Physics **96**, 1983 (2004).

[9]G. Freychet, P. Naulleau, R. Pandolfi, D. Kumar, J. Strzalka, D. Sunday, A. Hexemer, J. R. Kline, D. Staacks, and M. Fukuto, in *Metrology, Inspection, and Process Control for Microlithography XXXII*, edited by O. Adan and V. A. Ukraintsev (SPIE, San Jose, United States, 2018) p. 37.

[10]G. R. Muthinti, B. Peterson, R. K. Bonam, and A. C. Diebold, Journal of Micro/Nanolithography, MEMS, and MOEMS **12**, 013018 (2013); A. Faridian, V. F. Paz, K. Frenner, G. Pedrini, A. D. Boef, and W. Osten, *ibid.* **14**, 021104 (2015); D. Dixit, S. O'Mullane, S. Sunkoju, A. Gottipati, E. R. Hosler, V. Kamineni, M. Preil, N. Keller, J. Race, G. R. Muthinti, and A. C. Diebold, *ibid.* **14**, 031208 (2015).

[11]R. Kizu, I. Misumi, A. Hirai, K. Kinoshita, and S. Gonda, Meas. Sci. Technol. **29**, 075005 (2018); H. Dohi and P. Kruit, Ultramicroscopy **189**, 1 (2018); Y. B. Zou, M. S. S. Khan, H. M. Li, Y. G. Li, W. Li, S. T. Gao, L. S. Liu, and Z. J. Ding, Measurement **123**, 150 (2018); R. K. Attota, H. Kang, K. Scott, R. Allen, A. E. Vladar, and B. Bunday, Meas. Sci. Technol. **29**, 125007 (2018).

[12]C. G. Shull and E. O. Wollan, Science **108**, 69 (1948); G. L. Price, in *Surface Analysis Methods in Materials Science*, edited by D. J. O'Connor, B. A. Sexton, and R. S. C. Smart (Springer Berlin Heidelberg, Berlin, Heidelberg, 2003) pp. 307–318.

[13]A. Ichimiya and P. I. Cohen, *Reflection High-Energy Electron Diffraction*, 1st ed. (Cambridge University Press, Cambridge, U.K. ; New York, 2004).

[14]A. Ichimiya, Japanese Journal of Applied Physics **22**, 176 (1983); M. G. Moharam and T. K. Gaylord, J. Opt. Soc. Am. A, JOSAA **3**, 1780 (1986).

[15]Python 3.6, http://www.python.org; T. E. Oliphant, *A guide to Numpy* (Trelgol Publishing, USA, 2006); E. Jones, T. Oliphant, P. Peterson, and others, *SciPy: Open source scientific tools for Python* (2001); Any mention of commercial products is for information only; it does not imply

recommendation or endorsement by NIST.

[16] Y. C. Wang, T. M. Chou, M. Libera, and T. F. Kelly, Applied Physics Letters **70**, 1296 (1997).

[17] J. I. Goldstein, D. E. Newbury, J. R. Michael, N. W. M. Ritchie, J. H. J. Scott, and D. C. Joy, *Scanning Electron Microscopy and X-Ray Microanalysis*, 4th ed. (Springer-Verlag, New York, 2018).

[18] L. H. Friedman and W-L Wu, United States Patent Application, Pub. No. 2019/0057834 A1, Pub. Date: Feb. 21, 2019.

Supplementary Material for

“Electron Reflectometry for Measuring Nanostructures on Opaque Substrates”

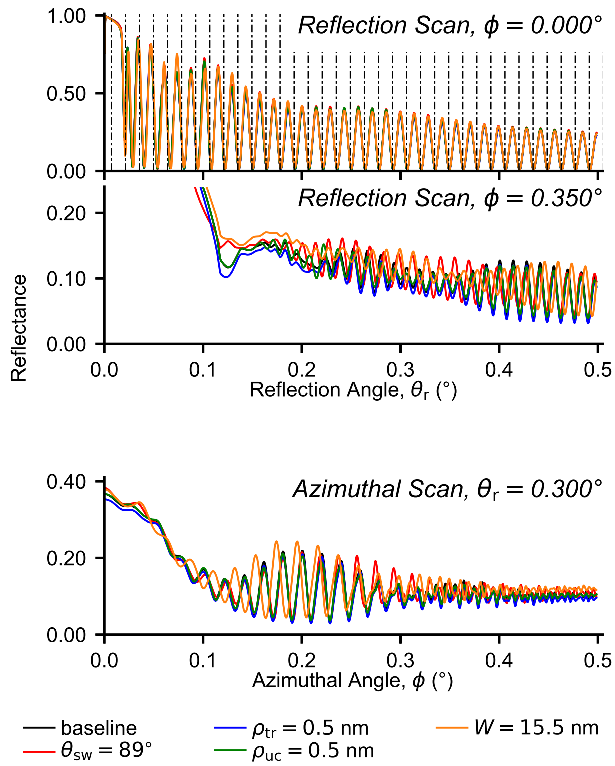

Figure S1. Dynamic simulations of ER scans of baseline and other gratings as in Fig. 3 and described in text, but incident beam and detection aperture diameters are finite; $d_i = d_d = 20\ \mu$m. Vertical dot-dashed lines indicate OPD-predicted reflectance minima. These small-aperture scans are virtually indistinguishable from ideal scans (Fig. 3)